Nanoscale Advances

ROYAL SOCIETY OF CHEMISTRY

PAPER

View Article Online
View Journal | View Issue

Cite this: *Nanoscale Adv.*, 2026, **8**, 1679

Analysis of the effects of plasma-generated active species on cells cultured in a microperfusion system

Hayata Okino and Shinya Kumagai *

Received 1st September 2025
Accepted 16th January 2026

DOI: 10.1039/d5na00841g

rsc.li/nanoscale-advances

Promoting cell growth is required in life science and medical applications. Thus far, microdevice researchers have been developing microperfusion systems for simulating *in vivo* conditions that are suited for cell growth. For advancing cell growth technology further, we applied plasma technology. Plasma is the fourth state of matter after solid, liquid, and gas. When plasma is generated under atmospheric conditions, it reacts with ambient air, producing reactive oxygen and nitrogen species (RONS), which affect cells. These RONS can be used as triggers for promoting cell growth. In this study, we achieved the delivery of RONS to the cells in a microperfusion system using simple methods. We evaluated plasma effects on cell growth and analyzed RONS propagation in a liquid medium for cells under microperfusion.

Introduction

Microperfusion systems have been developed for realizing stable cell cultures.[1–9] For promoting cell growth, cell culture chambers are now fabricated with 3D structures for simulating *in vivo* conditions. Thus, the culture technology enables the formation of 3D biomaterials, such as spheroids and organoids, as well as sheets of cells, which are formed by conventional 2D culture. These 2D and 3D cell materials are used in various applications, such as drug screening and as transplantation materials in regenerative medicine. However, processes of forming these bio-materials are time-consuming. Shortening cell culture time has been demanded for a long time to accelerate research activities in life science and medical treatments.

To advance cell culture technology further, we focused on "plasma". In biology, the term "plasma" is used to describe a substance filling the inside of cells and is also used to describe the liquid part of the blood. In contrast, in physics and technology, the term "plasma" is used to describe the fourth state of matter.[10] It is composed of positively and negatively charged particles and is an electrically neutral system, in which the positively and/or negatively charged particles are in thermal motion. Since plasma contains charged particles (ions and electrons) and chemically active species (radicals), plasma has various reactivities. One of the most successful applications is material processing. In particular, plasma technology has been used for microfabrication in semiconductor device production. In the microfabrication process, semiconductor materials are loaded into vacuum chambers. Then, reactive gases are supplied inside the chamber, and non-thermal plasma is generated to etch semiconductor materials or deposit thin films on a substrate.

With the advancement of plasma generation technology, non-thermal plasma has been made available under ambient conditions. When non-thermal plasma is generated under ambient conditions, the plasma reacts with ambient air, generating reactive oxygen species (ROS) and reactive nitrogen species (RNS), collectively known as reactive oxygen and nitrogen species (RONS). It is well known that RONS can affect the living bodies. Therefore, non-thermal plasma is applied to control the viability of biological samples, such as cells.[11–13] Optimizing the doses of RONS is the key to control the viability of cells. Thus, the non-thermal plasma has been used in the studies of sterilization,[14] wound treatments,[15–18] promotions of cell proliferation,[19] promotion of cell differentiation,[20–22] and gene transfection.[23,24] Many innovative results have been reported to date.

However, it is difficult to supply plasma-generated RONS to cells under microperfusion. Microperfusion requires a "closed" environment for flowing liquid medium [Fig. 1(a)], while plasma requires an "open" environment for generating RONS through reactions with ambient air [Fig. 1(b and c)]. Therefore, we must manage these contradictory conditions and supply RONS to the cells without disturbing the microperfusion culture.

Thus far, one of the authors has developed a microsystem which enables direct plasma exposure of cells cultured in microwells. The microsystem was referred to as "Plasma-on-Chip".[25–27] The Plasma-on-Chip was suited for conducting direct plasma exposure of single cells cultured in microwells. This is one of the merits of using Plasma-on-Chip, but microfabrication of the Si substrate is needed.

Meijo University, 1-501, Shiogamaguchi, Tempaku-ku, Nagoya, 468-8502, Japan. E-mail: skumagai@meijo-u.ac.jp

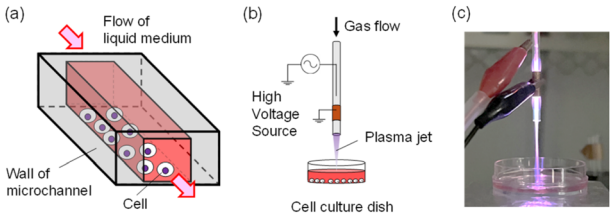

Fig. 1 (a) Perfusion cell culture is conducted under closed environments. (b) Plasma exposure of cells conducted under open-air environments. (c) An example of plasma exposure experiment.

In this study, we advanced Plasma-on-Chip technology to achieve plasma exposure of cells under microperfusion using simple methods. With the system developed here, we evaluated plasma exposure effects on cell proliferation in the microperfusion system. Also, we analyzed how plasma-generated active species propagate towards the cells in the microperfusion system.

Principle of plasma exposure of cells under microperfusion

To conduct plasma exposure of cells under microperfusion, a micro air–liquid interface is prepared at the bottom of the microchannel, as shown in Fig. 2. When liquid medium is injected into the microchannel, the surface tension of the liquid medium forms an air–liquid interface at the microgap.[25] The air–liquid interface holds the liquid medium without allowing it to leak to the outside. Next, a plasma generator is installed below the microgap. When a non-thermal atmospheric pressure plasma is generated, RONS are generated through the reaction with ambient air (O_2, N_2). The RONS diffuse towards the micro air–liquid interface, pass through the interface, propagate in the liquid medium, and finally reach the cells under microperfusion [Fig. 2(b)]. This principle can affect many cells under microperfusion, thereby fulfilling the demands of promoted cell growth in life science and medical applications.

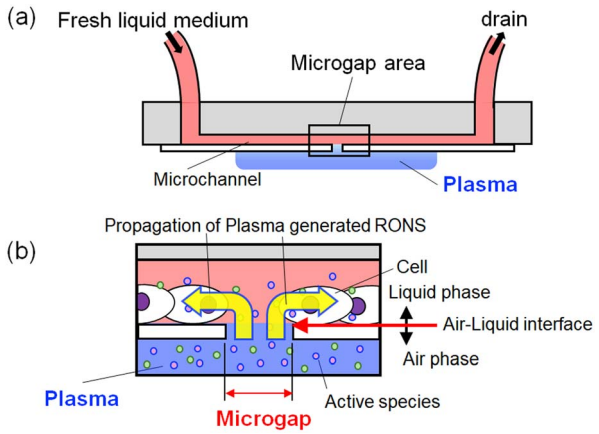

Fig. 2 Principle of plasma exposure of cells under microperfusion. (a) Cross-sectional drawing of the microperfusion system. A microgap is prepared at the bottom of a microchannel. (b) Magnified drawing of the microgap. The surface tension of the liquid medium forms an air–liquid interface, thereby holding the liquid medium without allowing it to leak to the outside. Passing through the air–liquid interface, plasma-generated RONS propagate in the liquid medium towards the cells.

Materials and methods

System structure of plasma exposure of cells under microperfusion

The microperfusion system consists of a microchannel device, a planar dielectric barrier discharge (DBD) plasma generator, a base holder, and a liquid medium delivery system (Fig. 3). The whole setup is designed to be set in a CO_2 incubator for stable cell culture.[9] Each component is described in the following sections.

Microchannel device

Details of the microchannel device fabrication were described in ref. 9. A microtrench device was fabricated through a molding process of poly-dimethylsiloxane (PDMS). Next, two glass plates are attached to each other at their side-edges [Fig. 4(a)] for making a microgap [Fig. 4(b)]. The microgap width is variable (5–50 μm) by adjusting the attaching force. Then, the microtrench PDMS device is set on the micro-gapped glass plates to form a closed microchannel [Fig. 4(c and d)].

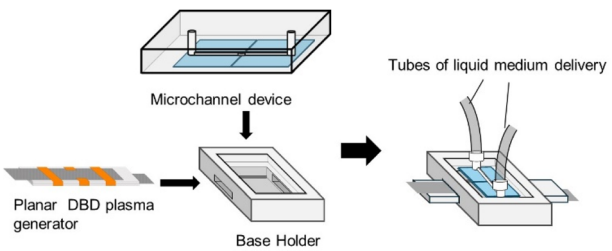

Fig. 3 Plasma exposure system for cells under microperfusion. The microchannel device and planar dielectric barrier discharge (DBD) plasma generator are installed in the base holder. Subsequently, tubes for the liquid medium delivery are connected.

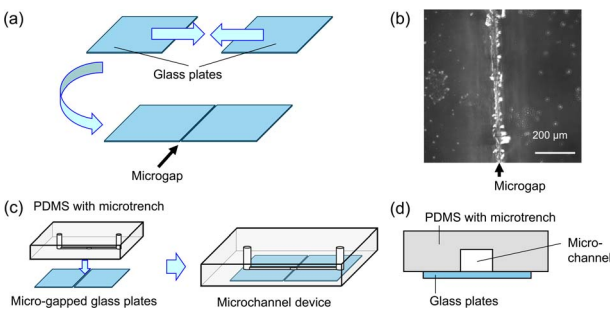

Fig. 4 Fabrication sequence of the microchannel device. (a) Glass plates are attached to each other at the side-edges to form a microgap. (b) Micrograph of the microgap formed between the glass plates. (c) PDMS with a microtrench installed on the micro-gapped glass plates to form a closed microchannel of perfusion cell culture. (d) Cross-section showing the microchannel formed.

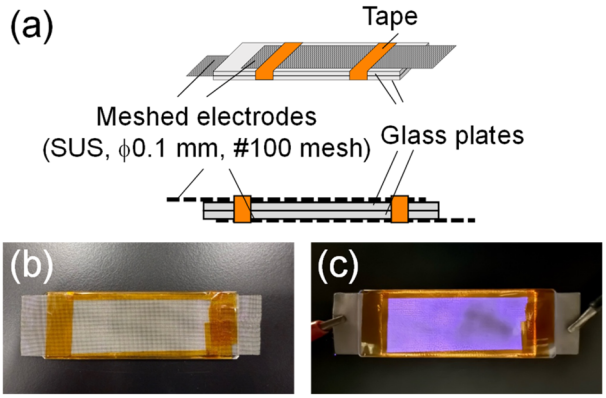

Fig. 5 (a) Schematic of the planar DBD plasma generator structure. Two slide glass plates (width: 76 mm, height: 26 mm, thickness: 1 mm) are stacked and sandwiched with meshed electrodes (SUS ϕ0.1 mm, mesh number: 100). (b) Planar DBD plasma generator. (c) Demonstration of plasma generation.

Planar DBD plasma generator

A planar DBD plasma generator was formed by sandwiching two glass plates (width: 76 mm, height: 26 mm, thickness: 1 mm) with meshed electrodes (SUS ϕ0.1 mm, mesh number: 100) (Fig. 5).[9] The meshed electrodes were made of SUS wires of ϕ0.1 mm (mesh number: 100). A high voltage power supply (LHV-09K, LOGY ELECTRIC, Japan) was connected to the meshed electrodes. When high voltage (9 kV, 15 kHz) was supplied to the plasma generator, a planar DBD plasma was generated.[9,28,29]

The voltage and current waveforms of the planar DBD plasma generator were measured using a high-voltage probe (Tektronix P6015A) and a current monitor (Model 6585, Pearson Electronics, USA), as shown in Fig. 6. Using the waveform data, the average power P of the plasma generator was calculated from eqn (1):

$$P = \frac{1}{T}\int_0^T V(t) \times I(t)\mathrm{d}t, \quad (1)$$

where V is voltage, I is current, and T is period.[30] The calculated power was 0.2 W cm^{-2}.

Generation of reactive oxygen and nitrogen species was confirmed using test strips (Quantofix Peroxide 25, Nitrate/Nitrite, MACHEREY-NAGEL, Germany). We detected hydrogen peroxide, nitrite, and nitrate as reported in ref. 9.

Base holder

A base holder was fabricated by 3D printing. The microchannel device and planar DBD plasma generator were assembled into the base holder.

Liquid medium delivery system

Two silicone tubes were connected to the microchannel device using luer fittings. One silicone tube was installed in a peristaltic pump (WSP-3300, ATTO, Japan) and used for supplying liquid medium. The other tube was used for flowing out the waste of liquid medium.

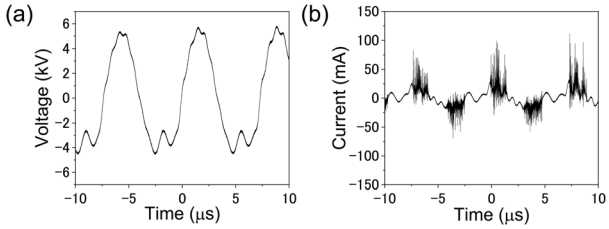

Fig. 6 Waveforms of (a) voltage and (b) current.

Cell culture

Murine myoblast cells C2C12 (RCB0987, RIKEN BRC, Japan) were used. After cell seeding into the system, microperfusion cell culture was conducted under the flow of liquid medium (DMEM with 10% FBS).

Murine fibroblast cells, L929 (ECACC, UK), were also used. L929 cells were cultured in a liquid medium (MEM with 10% FBS).

Plasma exposure of cells

C2C12 or L929 cells were injected into the microperfusion system and incubated for 24 h. During the incubation, the injected cells adhered to the bottom surface of the micro channel (*i.e.* surface of glass plate). The cells were observed by phase contrast microscopy, and the numbers of the cells were counted.

Then, plasma exposure was conducted. To clearly analyze plasma exposure effects, microperfusion was stopped. After 24 and 48 h of incubation, the numbers of cells were counted from the phase contrast microscopy images. Using the cell counts, proliferation ratios were calculated with respect to the numbers of cells before plasma exposure (*i.e.* 24 h after cell injection).

Visualization of liquid flow

To visualize liquid flow, a suspension of tracer particles (L4530, Sigma-Aldrich, USA; diameter: 2.0 μm) was injected into the microchannel. The liquid medium delivery system was suspended, thereby causing no perfusion flow. Upon plasma exposure through the micro air–liquid interface (microgap), the motions of tracer particles were observed with a fluorescence microscope (excitation: 470 nm, emission: 505 nm) equipped with a CCD camera. After movies of tracer particles were recorded, the movies were transformed into 8-bit images, and the motions of tracer particles were extracted clearly by appropriately setting the threshold level of brightness. Then, the trajectories of tracer particles were tracked and visualized using ImageJ software.[31,32]

Visualization of propagations of plasma-generated active species

To detect the propagation of plasma-generated active species, methyl red solution was used. Methyl red solution (Kishida Co.

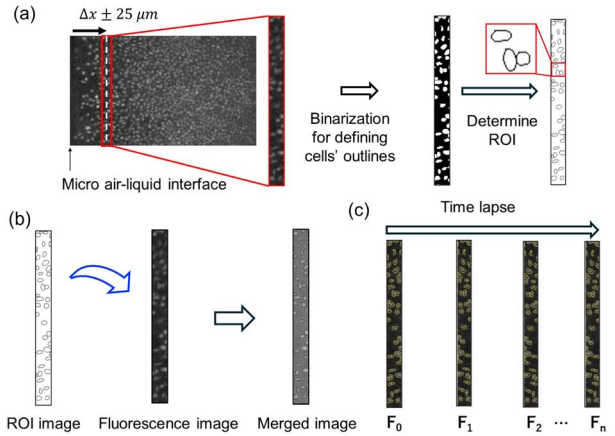

Fig. 7 Procedure of image analysis. (a) Determination of ROI. (b) Merged images of ROI and fluorescence microscopy for extracting fluorescence intensity data. (c) Variations in fluorescence intensities with time.

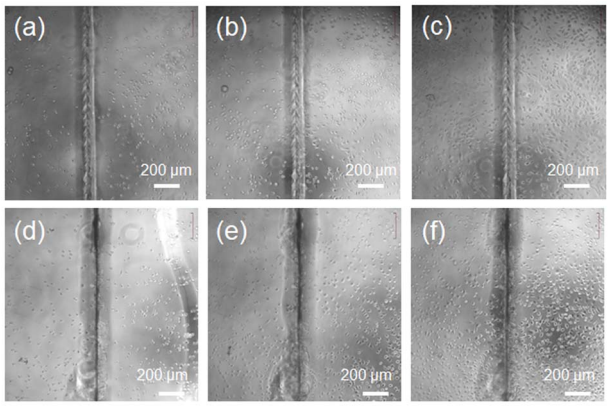

Fig. 9 Micrographs of C2C12 cells cultured in our microperfusion system: (a–c) without plasma exposure (control) and (d–f) with plasma exposure (exposure time 5 s). To clearly analyze plasma exposure effects, perfusion flow was stopped. Incubation time of (a and d) 0 h, (b and e) 24 h, and (c and f) 48 h.

Ltd, Japan), undiluted, was injected into the microchannel. Then, plasma exposure was conducted, and the solution color change from yellow to red was monitored. Methyl red exhibits a yellow color for pH values larger than 6.2 and a red color for pH values smaller than 4.2. In the intermediate range between pH 4.2 and pH 6.2, methyl red solution exhibits an orange color.

Visualization of propagations of plasma effects on cells under microperfusion

It is well known that the Ca^{2+} concentration in a cell changes upon external stimulation. The change of the Ca^{2+} concentration can be detected with a fluorescent probe. The fluorescent probe Fluo 4 AM (DOJINDO, Japan) was injected into the microchannel. Under excitation at 495 nm, Fluo 4 AM emits fluorescence at 518 nm.

The microperfusion system was set on the stage of an upright microscope. After plasma exposure, fluorescence intensity changes of C2C12 cells were monitored using a color CCD camera (WRAYCAM-VEX830, Wraymer, Japan).

To analyze the propagation of plasma-generated active species from the micro air–liquid interface (microgap), image analysis was conducted spatiotemporally using the ImageJ software, as shown in Fig. 7.[31,32] We focused on positions of 200, 400, 600, 800, and 1000 μm from the micro air–liquid interface (microgap). At each position, we set a rectangular region (range: ±25 μm). Color images acquired were transformed into gray scale. Then, image binarization was conducted to extract outlines of cells, and the region of interest (ROI) of each cell was defined. At each ROI, fluorescence intensity F was extracted. Then, the intensity change ΔF was calculated with respect to the fluorescence intensity at an elapsed time of 0 s and normalized as $(F - F_0)/F_0$. Changes of $(F - F_0)/F_0$ were analyzed as a function of elapsed time after plasma exposure.

Results and discussion

The assembled microperfusion system is shown in Fig. 8(a). The generation of DBD plasma is demonstrated in Fig. 8(b). The microperfusion system can be set in a CO_2 incubator with liquid reservoirs of fresh medium and waste products.

C2C12 cells were seeded in the microchannel. Under the microperfusion culture, we observed C2C12 cell proliferation in DMEM with 10% FBS and differentiation into tubular structures in DMEM with 2% HS, as reported in ref. 9.

Micrographs of cells cultured in the system are shown in Fig. 9. For both conditions without plasma exposure (control)

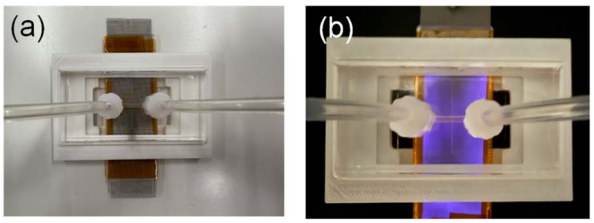

Fig. 8 (a) Microperfusion system. (b) Demonstration of the system operation. Blue and/or purple emissions of the DBD plasma are shown.

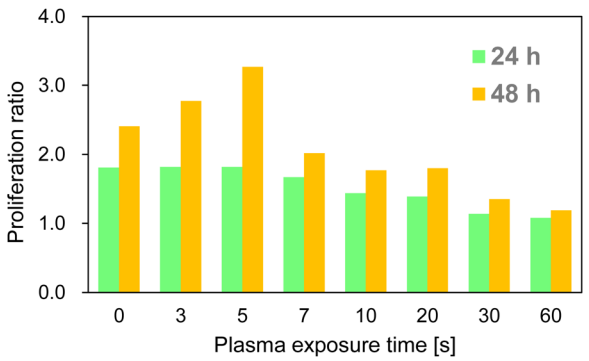

Fig. 10 Proliferation of cells for various plasma exposure times. For the exposure time of 5 s, the proliferation ratio increased by 1.4 times.

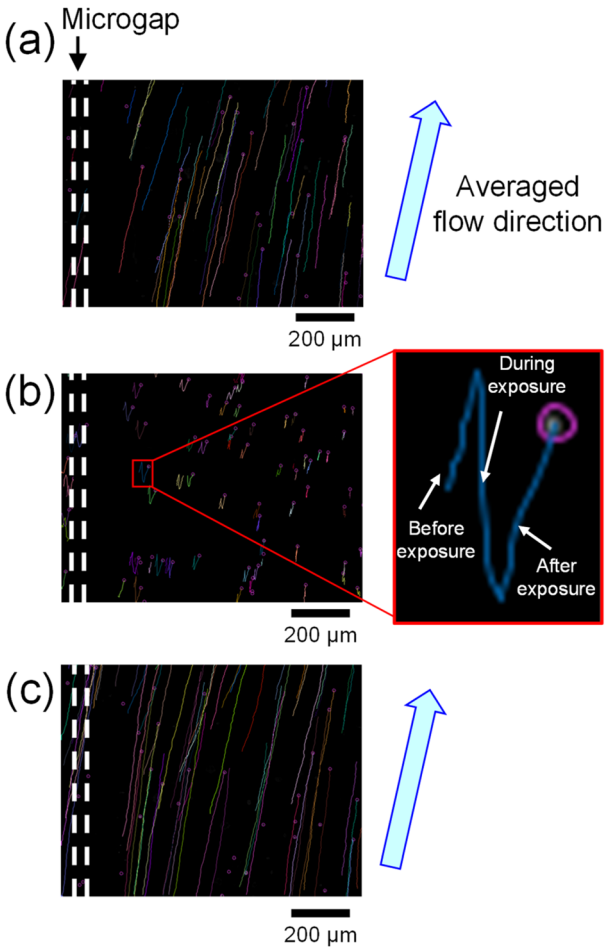

Fig. 11 Liquid flows visualized by tracer particles: (a) before plasma exposure (tracking duration is 175 s), (b) during plasma exposure of 10 s (tracking lines including 10 s before and after plasma exposure); the inset is a magnified image of a tracked particle, and (c) after plasma exposure (tracking duration is 175 s).

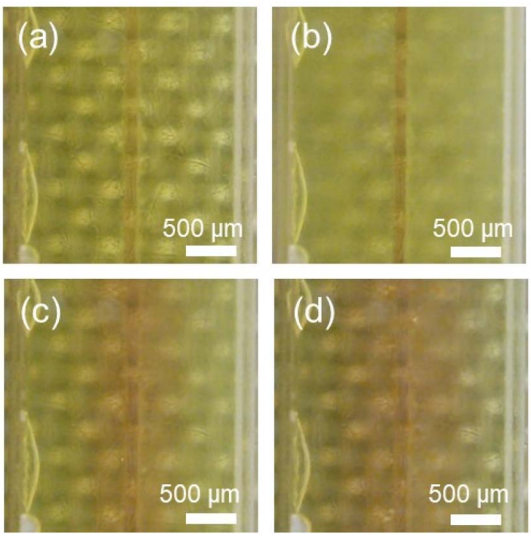

Fig. 12 Color changes of methyl red solution: (a) just after plasma exposure (0 s) and (b) 10 s, (c) 140 s, and (d) 300 s after plasma exposure.

and with plasma exposures (5 s), proliferation of cells was observed.

We analyzed the effects of plasma exposure time for cell proliferation (Fig. 10). Compared with control conditions (plasma exposure time: 0 s), enhancement of cell proliferation was observed until the plasma exposure time increased to 5 s. An enhancement of 1.4-fold was observed. However, with a further increase in plasma exposure time, the proliferation ratio decreased. Longer plasma exposure time was harmful to cells. From the results, plasma exposure of less than 5 s was

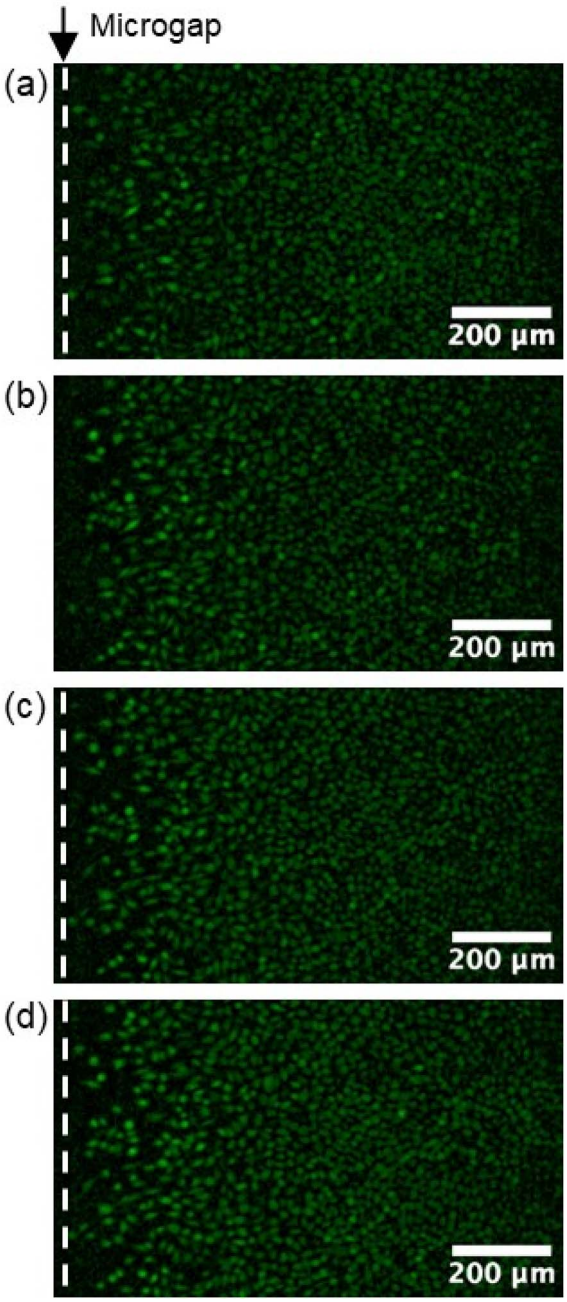

Fig. 13 Ca^{2+} imaging of L929 cells: (a) just after plasma exposure (0 s) and (b) 60 s, (c) 90 s, and (d) 600 s after plasma exposure. Fluorescence intensity changes propagated to deeper areas from the air–liquid interface as time passed.

suited for promoted cell growth. After 3 days of culture, cell density finally reached confluence.

To consider the plasma effects on cells, measurements of the propagation of plasma-generated RONS were conducted. First, the liquid medium delivery system was stopped. Motions of the tracer particles were analyzed under no perfusion flow. Therefore, the tracer particles reflect the convection flow of the liquid. The flow direction before plasma exposure is shown by an arrow, as shown in Fig. 11(a). As shown in Fig. 11(b), during plasma exposure, the flow direction changed suddenly. Surprisingly, it was observed that the flow direction was along the microgap. The liquid flow induced by plasma exposure did not effectively work to propagate the particles to the deeper area of the microchannel. After plasma exposure was stopped, the flow direction recovered to the original flow direction [Fig. 11(c)].

In contrast, in the methyl red solution experiments, as shown in Fig. 12, the red-colored area expanded from the micro air–liquid interface (microgap). The color-changed area appeared symmetrically from the air–liquid interface. The expansion of the color-changed area should reflect the diffusion of protons (local pH change) and/or the color-changed methyl red itself. At 300 s after plasma exposure, the area reached about 500 μm area from the air–liquid interface.

From the above results of Fig. 10 and 11, it is considered that plasma-generated active species propagated to the deeper area of the microchannel by diffusion due to concentration gradients.

Next, we conducted Ca^{2+} imaging of L929 cells after plasma exposure (Fig. 13). In this method, the propagation of plasma-generated active species can be detected by using the cells themselves as markers. Just after plasma exposure (0 s), L929 cells in the vicinity of the micro air–liquid interface (microgap) showed enhanced fluorescence. At 60 s after plasma exposure, the area of fluorescence shifted to a further deep area of the microchannel.

Time-lapses images were captured for each position (200, 400, 600, 800, and 1000 μm from the micro air–liquid interface (microgap)). The time-lapses images were processed and ratios of fluorescence intensity change $(F - F_0)/F_0$ were calculated as shown in (Fig. 14). At each point, the intensity change ratio increased to 60 s. Especially, the increasing tendencies were clearly observed for positions of 200, 400, and 600 μm.

Considering the results of the induced flow (Fig. 11) and concentration diffusion (Fig. 12), the propagation of fluorescence change was slightly faster. There were two possibilities. One is that some plasma-generated reactive species diffused faster than the reactive species which changed methyl red solution color. The other possibility is that signal transfer between cells propagated slightly faster to the deep area of the microchannel. After 60 s, the tendencies changed to a gradual increase. Since the Ca^{2+} imaging was conducted on the stage of a microscope, this gradual increase may have resulted from the factors related to uncontrolled environments.

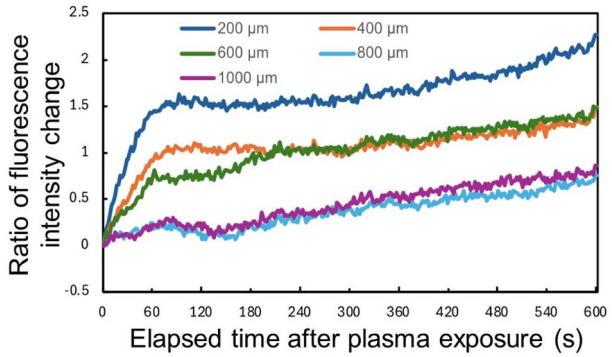

Fig. 14 Ratio of fluorescence intensity change $(F - F_0)/F_0$ as a function of elapsed time after plasma exposure for the positions of 200, 400, 600, 800, and 1000 μm from the micro air–liquid interface (microgap).

Conclusions

In this study, we developed a plasma exposure system for cells under microperfusion. To conduct plasma exposure of cells cultured in a closed microchannel, we created a micro air–liquid interface in the microchannel for supplying plasma-generated active species to cells. Under plasma exposure of less than 5 s, proliferation of C2C12 cells was observed. To analyze delivery of plasma-generated active species, we analyzed liquid flow induced by plasma exposure. From the results, the liquid flow induced by plasma exposure was small and the liquid flow did not work effectively for propagating plasma-generated active species to the deeper area of the microchannel. Considering the results of methyl red solution, plasma-generated active species were delivered by diffusion due to concentration gradients.

The microperfusion system developed here will contribute to activating research in life science and medical applications as well as plasma science.

Author contributions

Hayata Okino: performed the experiments; analyzed and interpreted the data. Shinya Kumagai, PhD: conceived and designed the experiments; performed the experiments; analyzed and interpreted the data; contributed reagents, materials, analysis tools or data; and wrote the manuscript.

Conflicts of interest

There are no conflicts to declare.

Data availability

The data supporting the findings of this study are included within the article.

Acknowledgements

This study was partially supported by the Takahashi Industrial and Economic Research Foundation and the joint usage/research program of Center for Low-temperature Plasma

Sciences, Nagoya University, Japan. Murine myoblast cell line, C2C12 (RCB0987), was provided by the RIKEN BRC through the National Bio-Resource Project of the MEXT, Japan.

References

1 K.-I. Kamei, Y. Kato, Y. Hirai, S. Ito, J. Satoh, A. Oka, T. Tsuchiya, Y. Chen and O. Tabata, *RSC Adv.*, 2017, **7**, 36777.
2 D. Zhang, J. Yang, Y. Hirai, K. Kamei, O. Tabata and T. Tsuchiya, *Jpn. J. Appl. Phys.*, 2023, **62**, 017002.
3 C. Heuer, J.-A. Preuß, T. Habib, A. Enders and J. Bahnemann, *Eng. Life Sci.*, 2022, **22**, 744.
4 A. R. Vollertsen, S. A. ten Den, V. Schwach, A. van den Berg, R. Passier, A. D. van der Meer and M. Odijk, *Biomed. Microdevices*, 2021, **30**, 23.
5 J. Dornhof, J. Kieninger, H. Muralidharan, J. Maurer, G. A. Urbana and A. Weltin, *Lab Chip*, 2022, **22**, 225.
6 G. Agrawal, A. Ramesh, P. Aishwarya, J. Sally and M. Ravi, *Biotechnol. Prog.*, 2021, **37**, e3126.
7 A. Garziano, F. Urciuolo, G. Imparato, F. Martorina, B. Corrado and P. Netti, *Lab Chip*, 2016, **16**, 855.
8 S. Parlato, G. Grisanti, G. Sinibaldi, G. Peruzzi, C. M. Casciola and L. Gabriele, *Lab Chip*, 2021, **21**, 234.
9 H. Okino, *et al.*, Microperfusion cell culture system for promoted cell growth using non-thermal atmospheric pressure plasma exposure, *Jpn. J. Appl. Phys.*, 2023, **62**, SG1043.
10 M. A. Liberman and A. J. Lichtenberg, *Principles of Plasma Discharges and Materials Processing* (Wiley, New York, 1994).
11 S. Toyokuni *et al.*, *Plasma Medical Science*, Academic Press, 2018.
12 D. B. Graves, *J. Phys. D: Appl. Phys.*, 2012, **45**, 263001.
13 K. Ishikawa, K. Takeda, S. Yoshimura, T. Kondo, H. Tanaka, S. Toyokuni, K. Nakamura, H. Kajiyama, M. Mizunog and M. Hori, *Free Radical Res.*, 2023, **57**, 239–270.
14 E. Stofels, Y. Sakiyama and D. B. Graves, *IEEE Trans. Plasma Sci.*, 2008, **36**, 1441–1457.
15 G. Fridman, G. Friedman, A. Gustol, A. B. Shelhter, V. N. Vasilets and A. Fridman, *Plasma Process Polym*, 2008, **5**, 503–533.
16 G. Isbary, G. Morfill, H. U. Schmidt, M. Georgi, K. Ramrath, J. Heinlin, S. Karrer, M. Landthaler, T. Shimizu, B. Steffes, W. Bunk, R. Monetti, J. L. Zimmermann, R. Pompl and W. Stolz, *Br. J. Dermatol.*, 2010, **163**, 78–82.
17 G. Isbary, J. Heinlin, T. Shimizu, J. L. Zimmermann, G. Morfill, H.-U. Schmidt, R. Monetti, B. Steffes, W. Bunk, Y. Li, T. Klaempfl, S. Karrer, M. Landthaler and W. Stolz, *Br. J. Dermatol.*, 2012, **167**, 404–410.
18 T. Shimizu, *Jpn. J. Appl. Phys.*, 2020, **59**, 120501.
19 Y. Hori, N. Iwata, V. Gamaleev, J.-S. Oh, T. Murata, M. Hori and M. Ito, *Plasma Processes Polym.*, 2021, **18**, e2000225.
20 M. Kobayashi, K. Tomoda, H. Morihara, M. Asahi, T. Shimizu and S. Kumagai, *Heliyon*, 2022, **8**, e12009.
21 K. Saito, H. Toyoda, M. Okada, J.-S. Oh, K. Nakazawa, Y. Ban, K. Orita, A. Shimatani, H. Yao, T. Shirafuji and H. Nakamura, *PLoS One*, 2024, **19**(4), e0298086.
22 Z. Xiong, S. Zhao, X. Mao, X. Lu, G. He, G. Yang, M. Chen, M. Ishaq and K. Ostrikov, *Stem Cell Res.*, 2014, **12**, 387–399.
23 M. Leduc, D. Guay, R. L. Leask and S. Coulombe, *New J. Phys.*, 2009, **11**, 115021.
24 M. Jinno, Y. Ikeda, H. Motomura, Y. Isozaki, Y. Kido and S. Satoh, *Plasma Sources Sci. Technol.*, 2017, **26**(9pp), 065016.
25 S. Kumagai, C.-Y. Chang, J.-H. Jeong, M. Kobayashi, T. Shimizu and M. Sasaki, *Jpn. J. Appl. Phys.*, 2016, **55**, 01AF01.
26 T. Okada, C.-Y. Chang, M. Kobayashi, T. Shimizu, M. Sasaki and S. Kumagai, *Arch. Biochem. Biophys.*, 2016, **605**, 18.
27 J.-S. Oh, S. Kojima, M. Sasaki, A. Hatta and S. Kumagai, *Sci. Rep.*, 2017, **7**, 41953.
28 R. Brandenburg, *Plasma Sources Sci. Technol.*, 2017, **26**, 053001.
29 X. Xu, *Thin Solid Films*, 2001, **390**, 237.
30 J.-S. Oh, E. J. Szili, N. Gaur, S. H. Hong, H. Furuta, R. D. Short and A. Hatta, *J. Photopolym. Sci. Technol.*, 2015, **28**, 439–444.
31 M. D. Abramoff, P. J. Magalhaes and S. J. Ram, *Biophotonics Int.*, 2004, **11**, 36–42.
32 C. A. Schneider, W. S. Rasband and K. W. Eliceiri, *Nat. Methods*, 2012, **9**, 671–675.